

# Interstellar Scintillation of Pulsar B0809+74

B. J. Rickett<sup>1</sup>, Wm. A. Coles<sup>2</sup>

*Department of Electrical and Computer Engineering, University of California, San Diego, CA 92093*

Jussi Markkanen<sup>3</sup>

*EISCAT-Geophysical Observatory, SF-99600 Sodankylä, Finland*

## ABSTRACT

Weak interstellar scintillations of pulsar B0809+74 were observed at two epochs using a 30m EISCAT antenna at 933 MHz. These have been used to constrain the spectrum, the distribution and the transverse velocity of the scattering plasma with respect to the local standard of rest (LSR). The Kolmogorov power law is a satisfactory model for the electron density spectrum at scales between  $2 \times 10^7$ m and  $10^9$ m. We compare the observations with model calculations from weak scintillation theory and the known transverse velocities of the pulsar and the Earth. The simplest model is that the scattering is uniformly distributed along the 310 pc line of sight ( $l = 140^\circ$ ,  $b = 32^\circ$ ) and is stationary in the LSR. With the scattering measure as the only free parameter, this model fits the data within the errors and a range of about  $\pm 10$  km s<sup>-1</sup> in velocity is also allowed. The integrated level of turbulence is low, being comparable to that found toward PSR B0950+08, and suggests a region of low local turbulence over as much as  $90^\circ$  in longitude including the galactic anti-center. If, on the other hand, the scattering occurs in a compact region, the observed time scales require a specific velocity-distance relation. In particular, enhanced scattering in a shell at the edge of the local bubble, proposed by Bhat et al. (1998), near 72 pc toward the pulsar, must be moving at about  $\sim 17$  km s<sup>-1</sup>; however, the low scattering measure argues against a shell of enhanced scattering in this direction. The analysis also excludes scattering in the termination shock of the solar wind or in a nebula associated with the pulsar.

*Subject headings:* scattering — plasmas — ISM: kinematics and dynamics — turbulence — radio continuum: ISM — pulsars: individual (B0809+74)

---

<sup>1</sup>e-mail: rickett@ece.ucsd.edu

<sup>2</sup>e-mail: coles@ece.ucsd.edu

<sup>3</sup>e-mail: jussi@eiscat.sgo.fi

## 1. Introduction

The use of pulsar scintillation to probe the interstellar medium has been complicated by the fact that most observations below about 1 GHz are in the strong scintillation regime. In this regime there are both refractive and diffractive components in the intensity scintillation pattern, and neither spatial scale is known a priori. Furthermore the contributions from various locations along the path of propagation do not add in a simple linear fashion (see Rickett, 1990 and Narayan, 1992 for reviews). Weak scintillation is much simpler to interpret since contributions from various locations add linearly and the spatial scale of each contribution depends only weakly on unknown parameters such as the spectral exponent and the inner scale. The temporal scale of each contribution depends primarily on its distance and its velocity. In principle, it is feasible to “invert” the observations to estimate the spatial spectrum of the electron density and, by exploiting the variable velocity of the Earth, to investigate distribution of the scattering plasma and its velocity.

Observations can be made in weak scintillation by using higher frequencies and/or nearby pulsars. However it is difficult to obtain a stable estimate of the covariance function because the time scale of the scintillation is of the order of an hour. Thus a given observation will typically contain only a few time scales. Earlier observations by Backer (1975) at 3 GHz and Malofeev et al (1996) at 3, 5 and 8 GHz have confirmed that weak scattering occurs more or less as expected, but have not been long enough to provide the statistical accuracy necessary for detailed model fitting.

In this paper we report two longer measurements of a circumpolar pulsar in weak scintillation. The temporal statistics of these data sets are adequate to estimate the spectrum over a decade in wavenumber and put constraints on the distribution and velocity of scattering plasma. We have developed a procedure for the analysis that may be more generally useful.

## 2. Observations and Data Analysis

The pulsar B0809+74 was selected because earlier observations at lower frequencies suggested that it should be in weak scintillation at 933 MHz, which is the only frequency available on the 30m EISCAT antenna at Sodankylä, Finland, and because it is circumpolar at that latitude (68N). The receiver

passband is 8 MHz centered on 933 MHz and one linear polarization was used. The use of one linear polarization introduces a potential bias in the analysis since the pulsar is partially polarized. As a result the apparent flux varies due to the rotation of the antenna and the Faraday rotation in the ionosphere. This was thought to be negligible at 933 MHz, but was later found to be important. The effect was eliminated by selecting an unpolarized portion of the pulse profile as discussed below.

Impulsive interference is common at Sodankylä and the square law detector was designed to reduce the contribution from very short noise pulses. The pulsar intensity could be adequately sampled at 100 samples per sec (sps), however it was actually sampled at 100 Ksps using a very broad band detector. Pulses exceeding about 10 standard deviations were clipped at the sampler. The 100 Ksps series was then smoothed and decimated by a factor of 1000. This process reduced the contribution of impulsive interference to a low level without distorting the pulsar signal, and also reduced the rms quantization noise by a factor of 30. We observed continuously for 75 hours starting at 20 hr UT on 1996 April 8, although the observations were stopped due to system errors and restarted several times. We also observed a second epoch from 23 hr UT on 1998 September 30 for 85 hrs.

The data were summed (off-line) according to the apparent pulsar period (Doppler-shifted to the observatory). Each period ( $\approx 1.29$  s) was tested for interference using the ratio of the rms to the mean off-pulse power. The expected value of this ratio is about 0.003 and its standard deviation for a single pulse period is about 0.0003. Periods for which this ratio exceeded 0.005, about 7 standard deviations, were rejected. Successive integrations of the pulse profile were computed every 2 minutes. These were examined by hand and obvious interference was removed. The automatic interference test was very effective so less than 1% of the 2 minute averages were edited manually. Pulse profiles were also computed every 10 minutes. Both 2 and 10 minute averages were used in subsequent work. The average pulse profile was used to estimate the energy in an on-pulse window and also in an equal off-pulse window. First an estimate of the background power was subtracted, then the energy in each of the two windows was computed.

Initially we used an on-pulse window which included the entire pulse, however a referee, (Michael

Kramer), pointed out that B0809+74 has 30% linear polarization (Gould and Lyne, 1998). Examination of our pulse profiles revealed a 24 hr periodicity in the leading edge, which could be attributed to the linear polarization of the pulsar, the rotation of the telescope, and the diurnal change in the Faraday rotation in the ionosphere. This contributed about 10% of the variance in the pulse flux. Although this is not large it was greater than our estimation error and significantly altered our conclusions. The Gould and Lyne observations show strong linear polarization in the leading half of the pulse with no rotation of position angle, but the trailing half of the pulse is essentially unpolarized. Thus we changed our pulse energy computation to use a 50 msec on-pulse window starting at the pulse peak and including all the trailing half. With this window the polarization modulation was not detectable. The resulting time series of on-pulse power and off-pulse noise are displayed in Figure 1 with 10 minute resolution. The flux density was not calibrated absolutely, it has been normalized to unity averaged over the entire observing period.

In the absence of explicit flux density calibration, we used the variation of the system noise level to obtain a limit on the gain variation. The off pulse system noise varied almost regularly with a period of 24 hrs and an amplitude of about 6% peak to peak. We assume that most of this variation is due to changes in the atmospheric and ground noise contributions, as the zenith angle varied from  $6^\circ$  to  $38^\circ$  and the azimuth remained in the northern quadrant during the 24 hr period. We therefore conclude that the gain variation is periodic over 24 hr with an amplitude considerably less than 6% and thus is negligible compared to the large variations over a few hours observed in the pulse intensity.

The second order temporal statistics, i.e. the power spectrum and the autocovariance function, can be theoretically modelled and used to estimate the distribution of scattering material, its velocity and some characteristics of the turbulent spectrum. Although the two statistics are simply related by a Fourier transform, their estimation errors are quite different and both are useful for different purposes.

To estimate the time scale we computed the structure function rather than the autocovariance function, since the structure function is a more reliable estimator when the number of independent samples of the scintillations is not very large, as is the case here. For this purpose we used the 10 min

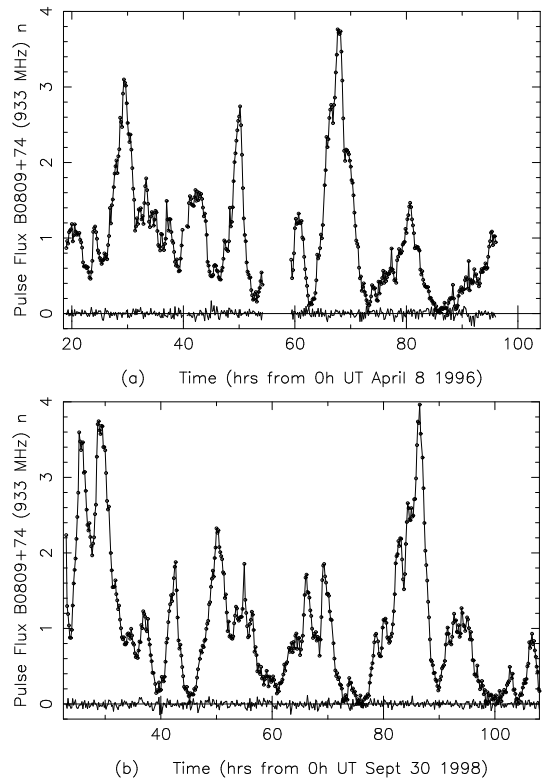


Fig. 1.— Observations of the total pulse flux of B0809+74 at 933 MHz, normalized to the mean flux over the observing period. The samples plotted are 10 minute averages. The lower traces are computed from an off-pulse window to provide a noise estimate. (a) Data from April 1996. (b) data from October 1998.

data because the noise correction for these data is negligible and the resolution is more than adequate. The structure function was computed in the usual way from the series of pulsar energies  $I_j$  (normalized by their estimated mean) sampled at times  $t_j$ .

$$\hat{D}_I(\tau_l) = \frac{\sum_l^{i,j} [I_i - I_j]^2}{\sum_l^{i,j} 1} \quad (1)$$

Here  $\sum_l^{i,j}$  represents the summation over all data pairs with time difference  $t_i - t_j$  lying within a window of width  $\delta p$  centered on  $\tau_l = l\delta p$ , where  $l$  is an integer and  $\delta p$  is the resolution of the data. The maximum lag computed was three quarters of the total duration of the observations.

Errors in the structure function result from additive receiver (radiometer) noise, intrinsic pulse to pulse variation, and from estimation errors due to the finite observing span. The receiver noise and intrinsic variation are effectively white and independent of the scintillation. They represent additive

constants in the structure function which can be subtracted. The receiver noise contribution can be estimated very accurately from the off-pulse noise. To measure the intrinsic variation we used the 2 min data. The first point in the structure function of the 2 min data is dominated by intrinsic variation and receiver noise. This was used to estimate the contribution of intrinsic variation to the structure function of the 10 min data with very good accuracy. The corrected structure function of the 10 min data is shown in Figure 2.

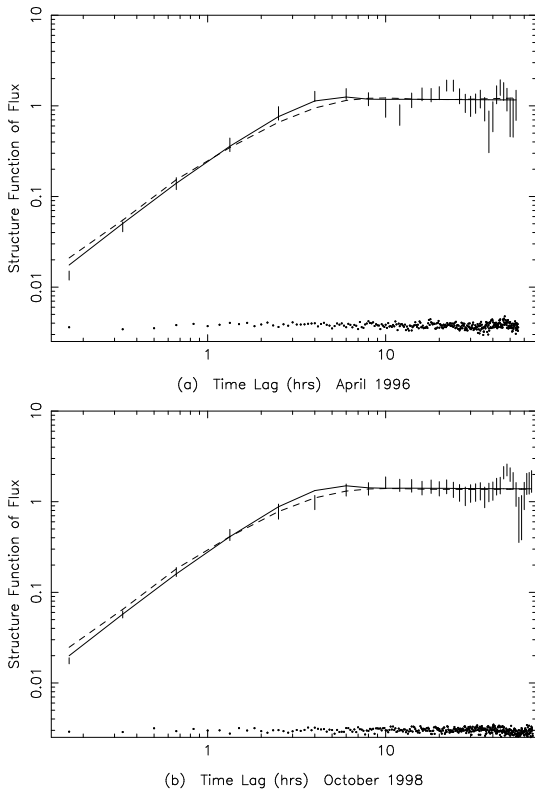


Fig. 2.— Structure functions of pulse flux time series shown in Figure 1 corrected for receiver noise and intrinsic variation. The data are marked by  $\pm\sigma$  error bars: (a) April 1996; (b) October 1998. The solid lines are the best fit theoretical models for a thin screen. The dashed lines are best fit models for a uniform extended scattering medium (as described in section 3.2). The dots represent the structure function of the receiver noise.

The estimation errors in the structure function due to the finite data length are substantial; they are derived in Appendix B. The  $\pm\sigma$  estimation errors, given by equation (B12), are indicated by the error bars in Figure 2. As discussed in the Appendix

the fractional error due to estimation error decreases toward small time lags but is partially compensated by the addition of the errors due to noise. The estimation errors are correlated over about an octave in time lag below saturation. At larger lags they are correlated over a characteristic time scale defined as the 50% width of the autocovariance. For model fitting purposes, the lags were decimated to reflect this distribution of independent estimates.

The power spectra were computed from the 2 min data using a direct Fourier transform procedure. The 1996 data was divided at the data gap and the two halves were transformed separately and their spectra added. The 1998 data was transformed in one block. The spectra were computed with a raw resolution of  $7.3 \times 10^{-3}$  cycles per hour (cph) and normalized so that the integral under the spectrum is the variance. They were boxcar smoothed and decimated by a factor which increased from 3 for the lowest 4 points to 125 for the highest frequencies. This reduces the estimation error and broadens the resolution. The white noise contribution from receiver noise and intrinsic variation was estimated from the frequencies above 5 cph, where the scintillation power is negligible, and subtracted from the spectral estimate. The final power spectra are plotted in Figure 3. The vertical bars indicate the  $\pm\sigma$  estimate error and the horizontal bars indicate the frequency resolution. Power spectra are convenient for model fitting, particularly at the high frequencies, because the estimation errors are independent and their variance is known. Thus it is easy to obtain reliable confidence intervals.

Two basic parameters which describe the flux time series are the normalized standard deviation or scintillation index  $m_w$ , and the time scale  $\tau_w$  at which the correlation function falls to 50%. They were derived from the structure function using the fact that  $D_I(\tau)$  saturates at  $2m_w^2$  for large time lags and estimating the time scale as the lag where  $D_I(\tau)$  crosses half the saturation level (i.e.  $D_I(\tau_w) = m_w^2$ ). By this method we found  $m_w = 0.77 \pm 0.2$  and  $\tau_w = 1.93 \pm 0.2$  hr for the 1996 observations and  $m_w = 0.84 \pm 0.15$ , and  $\tau_w = 2.19 \pm 0.2$  hr for the 1998 observations.

### 3. Model Fitting and Interpretation

Even though the observed scintillation indices ( $\approx 0.8$ ) are not much less than unity, we initially interpreted the results using weak scintillation theory. The advantage of weak scintillation theory is that

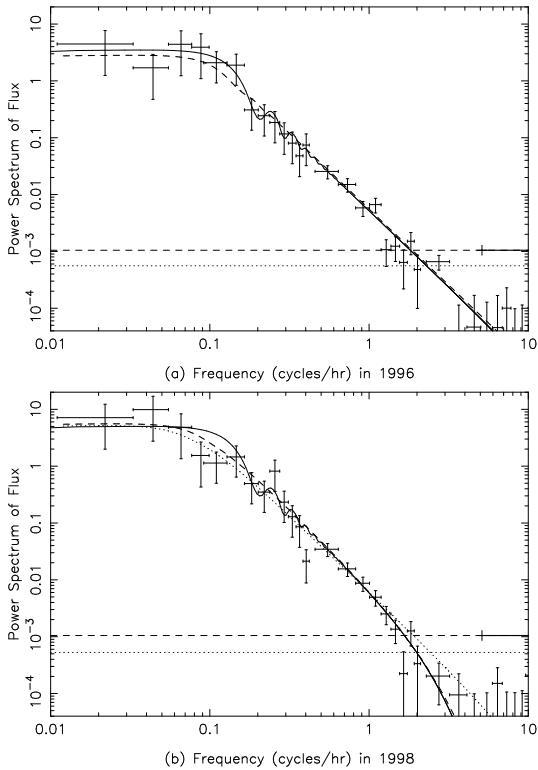


Fig. 3.— Power spectra of the pulse flux time series shown in Figure 1 corrected for receiver noise and intrinsic variation, (a) 1996 and (b) 1998. The data are marked by  $\pm\sigma$  error bars and the resolution is indicated by the horizontal bar. The off-pulse noise spectrum is marked by a dotted horizontal line. The sum of the off-pulse noise and the intrinsic noise is marked by a dashed horizontal line. The frequency range from which the intrinsic contribution was estimated is marked with a heavy horizontal line. The best fit theoretical models for a thin screen are shown by solid lines. The best fit theoretical models for a uniform medium which is stationary in the LSR are shown by dashed lines. The best fit models in 1996 have zero inner scale, but in 1998 they have  $s_i = 2 \times 10^7$  m. A best-fit theoretical model for a uniform medium with zero inner scale is also drawn over the 1998 data as a dotted line for comparison.

the observed structure functions and power spectra are linear integrals contributed from all points on the line of sight as described by the Born approximation discussed in Appendix A. Under weak scintillation we can do quantitative modelling of the density spectrum and the velocity distribution of the scattering medium. However when the scintilla-

tion index approaches unity, there can be significant departures from the linear Born model. Simulations by Frehlich (1999, private communication) corresponding to our observed  $m_w \approx 0.8$  show that the primary effect of incipient strong scattering is to broaden the spectrum by a factor of  $1.20 \pm 0.02$  and to reduce the time scale  $\tau_w$  by the same factor. The scintillation index  $m_w$  is also reduced by 4% from the weak scattering approximation. The statistical error in  $m_w$  is about 20% so the 4% bias due to incipient strong scintillation is negligible. However the statistical error in  $\tau_w$  is only 10%, so we have divided all our Born model calculations by the factor of 1.20 to ensure that the bias is less than the statistical error. Strong scattering also smoothes the “Fresnel ripples” in the spectrum and rounds the “knee” of the structure function, but this is a second order effect.

We assume that the density spectrum is an isotropic Kolmogorov power law, and also consider the effect of an inner scale. We need only consider one basic geometry: the pulsar is a point source at a distance  $L$  from the Earth and a thin scattering screen is located  $z_p$  from the pulsar and  $z_o$  from the earth, where  $z_p + z_o = L$ . To compute the temporal statistics we also need the velocity of the Earth, the pulsar, and the scattering screen. We can then compute the effect of a distribution of scattering material along the line of sight by integrating over all such elementary screens.

We have referred all velocities to the “local standard of rest” (LSR), since that appears to be the logical reference frame for the velocity of the interstellar plasma between the Earth and the pulsar. In this frame the solar velocity is  $20 \text{ km s}^{-1}$  directed towards right ascension of 18 hrs and declination of  $+30^\circ$ . The pulsar velocity ( $V_\alpha = 31 \pm 10 \text{ km s}^{-1}$ ;  $V_\delta = -55 \pm 9 \text{ km s}^{-1}$  in this frame) is determined from its proper motion (Lyne, Anderson, and Salter, 1982) and its distance (310 pc) from the model of Taylor and Cordes, 1993 [TC93].

In the following we will compare the observations with two models: (1) a single thin screen and (2) a uniform distribution. We find satisfactory agreement for both models, and then explore what range of LSR velocities is allowed for the scattering medium.

### 3.1. Thin Screen Model

The intensity structure function for weak scattering by a thin screen with a simple Kolmogorov

spectrum (equation A12), has the universal form (A13). The time scale  $\tau_w = 0.98 r_f/V_{\text{eff}}$ , where  $r_f = \sqrt{z_o z_p/Lk}$  is the ‘‘Fresnel scale’’, i.e. the spatial scale at the screen that contributes most of the scintillation, and  $V_{\text{eff}}$  is the velocity of the scattering plasma across the line of sight given by equation (A9). (It should be noted that the spatial scale at the observing plane is expanded by spherical divergence to  $r_f L/z_p$ ).

The best fit thin screen models are drawn over the observed structure functions as solid lines on Figure 2. The structure function at the smallest lag was excluded from the fit, in order to avoid the possible influence of an inner scale and because the correction for intrinsic pulse variation has uncertainties not reflected in the error bars at the smallest lag. As discussed earlier the lag values were chosen to sample approximately independent estimates and two parameters were fitted. This gave approximately 28 and 34 degrees of freedom, respectively in 1996 and 1998. The minimum  $\chi^2$  were 34 and 30, respectively, which indicates satisfactory fits to the data; the differences reflect the fact that the errors in the saturated portion of the structure functions are noticeably different in the two years. We use these fitted models to make refined estimates of the time scale and its errors:  $\tau_w = 1.99 \pm 0.18$  hr and  $\tau_w = 2.05 \pm 0.16$  hr for the 1996 and 1998 observations, respectively. These time scale estimates average over a range of time lags and so reduce the effect of the particular errors near where the structure function crosses half its saturation level. Hence we also use these same time scale estimates to characterize the data in section 3.2 on the extended medium model.

Weak scintillation theory predicts the relative contribution to the variance  $m_w^2$  and the Fresnel scale  $r_f$  for a screen at position  $0 < z_o < L$ , which are plotted in panels (a) and (c) of Figure 4. The effective velocity  $V_{\text{eff}}$  for the mean time of the 1996 observations is plotted as a solid line and that for the 1998 observations is plotted as a dashed line in panel (b) under the assumption that the scattering plasma is stationary with respect to the LSR. The predicted time scales  $\tau'_w = 0.82 r_f/V_{\text{eff}}$  (corrected for  $m_w = 0.8$ ) are plotted in the lower panel Figure 4(d) as a thick solid line for 1996 and a thick dashed line for 1998. The uncertainty limits in these time scales caused by errors in the pulsar proper motion are indicated by light solid and dashed lines at  $\pm\sigma$ . Also shown are the confidence intervals for the mea-

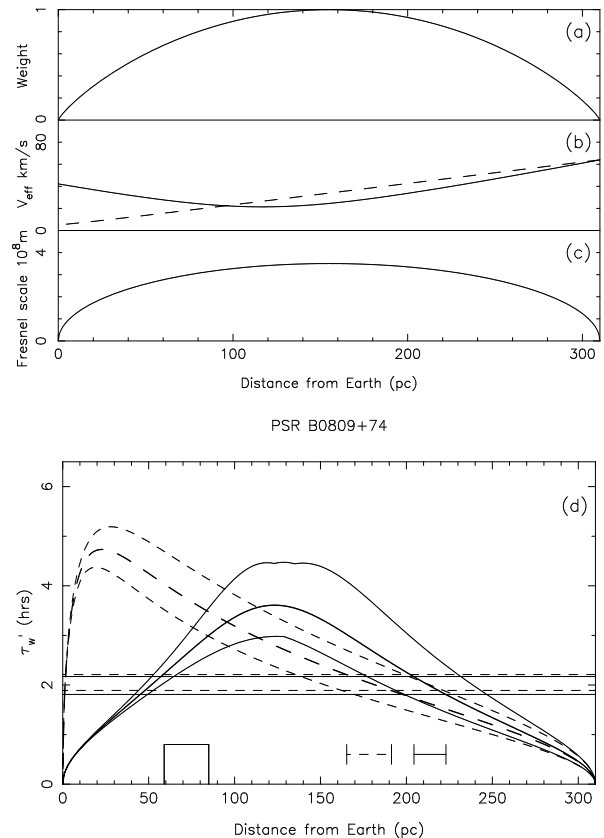


Fig. 4.— Dependence of weak scintillation parameters on screen distance: (a) contribution to variance; (b) effective velocity  $V_{\text{eff}}$  with respect to the LSR (solid line 1996, dashed 1998); (c) Fresnel scale; and (d) time scale (solid line 1996, dashed 1998). The time scales have been reduced by a factor 1.20 from the Born theory to account for incipient strong scattering. The thin lines show the envelope of time scales corresponding to errors in the pulsar proper motion. The confidence intervals for the observed time scale are shown as horizontal line pairs near 2 hrs (solid line 1996, dashed 1998). The bars indicate allowed distances to the screen at each epoch assuming the nominal pulsar velocity. The rectangle indicates the distance to the shell of enhanced scattering proposed by Bhat et al. (1998).

sured time scales as horizontal pairs of lines.

Neglecting the error in the proper motion for the moment, one can see that there are two locations at which a thin screen would provide the time scale measured in 1996, at  $51 \pm 6$  pc and  $213 \pm 9$  pc. After analyzing the 1996 observations we realized that this ambiguity could be resolved with addi-

tional observations at a different epoch (we thank Don Backer for pointing this out). Then the Earth's velocity would be different and so curves for  $V_{\text{eff}}(z_o)$  and  $\tau_w(z_o)$  would also be different. This is shown in Figure 5 where we plot  $V_{\text{eff}}(z_o)$  and  $\tau_w(z_o)$  for six observing epoch's spaced every two months on the 8th of each numbered month. One can see that the velocity near the pulsar does not change much but the velocity near the Earth changes dramatically. If the scattering screen were located near 213 pc, then the time scale would remain near 2 hrs. However if the scattering screen were located near 51 pc, the time scale would be much larger if observations were made between July and October. Accordingly we chose to reobserve the source in October 1998. One can see from Figure 4(d) that the 1998 observations are consistent with distances of  $1 \pm 0.1$  pc or  $178 \pm 12$  pc. The ambiguity is thus resolved in favor of the larger distance. However the match is not perfect as the  $\pm\sigma$  error bars do not overlap. The probability of this occurring by chance is less than 2% so we are led to consider the possibility that the medium may not be stationary in the LSR, which we discuss later in Section 4. We note that the uncertainty in screen location due to errors in the pulsar proper motion are larger than those due to errors in the measured time scale. Thus the two possible screen distances ( $213 \pm 9$  pc and  $178 \pm 12$  pc) are in fact jointly uncertain by about  $\pm 28$  pc. However, since the pulsar velocity must be the same at each epoch there is no single distance that matches both observations. It should also be noted that, in any case, it is very unlikely that the 1998 observations could have come from the closer location, because that would require a very thin, very intense scattering screen.

We also fit the simple Kolmogorov model with no inner scale to the estimated power spectra. The 1998 data were best fit with a nonzero inner scale (as described in section 3.3) but this did not affect the estimate of the time scale. The results,  $\tau_w = 1.84 \pm 0.22$  hr for 1996 and  $\tau_w = 1.84 \pm 0.15$  hr for 1998, are not quite consistent with the time scales derived from the structure functions. The confidence limits for the two methods just touch, suggesting that there may be a real bias. This could occur because the power spectra and the structure functions emphasize different aspects of the data. The structure function fit is dominated by scales near  $\tau_w$  whereas the power spectrum fit is dominated by the higher frequencies. The effect is that estimates from the power spectrum would move the location of the screen about 15 pc closer to the pul-

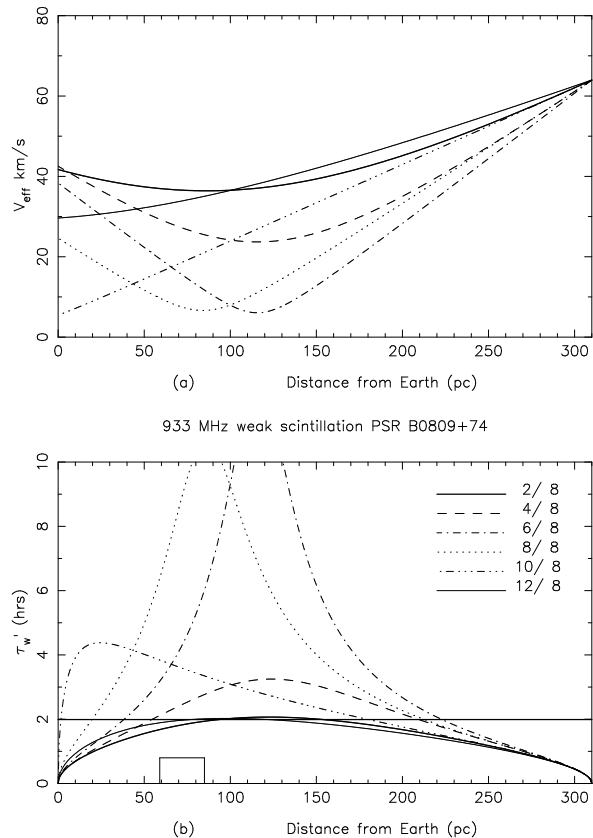


Fig. 5.— Dependence of weak scintillation parameters on screen distance plotted for six epochs as indicated by month/day: (a)  $V_{\text{eff}}$  with respect to the LSR; (b) Scintillation time scale (with 20% reduction to correct for incipient strong scattering).

sar. We use the time scales from the structure function in further analysis.

The plots of Figures 4 and 5 are based on models in which the screen is at rest in the LSR. In the Discussion (section 4) we consider models in which the screen is moving with respect to the LSR, and compare these with other astronomical information on motion in the local ISM. We now consider models with a uniform distribution of scattering.

### 3.2. Extended Scattering Model

When the scattering medium extends from the source to the observer, the theoretical structure function is the sum of many screen contributions each with an effective velocity  $V_{\text{eff}}(z_o)$  as in Appendix A. One can visualize this by looking at Figure 4; we add screen structure functions weighted by the curve in the top panel, with each structure

function scaled in time by the heavy curves in the bottom panel. We computed theoretical structure function for the 1996 and 1998 observing times assuming that the scattering plasma is uniformly distributed along the line of sight and is stationary in the LSR. As noted above we reduced the time lags by a factor of 1.20 in each model, to correct for the effect of incipient strong scattering. Then with the velocities known, the total variances  $m_w^2$  at each epoch are the only free parameters in the models. The corresponding least squares fits are plotted as dashed lines in Figures 2a and b. These models have a more rounded transition to saturation than for the screen geometry, and they fit the observed time scales reasonably well at half the saturation level. The  $\chi^2$  values for these fits are 39 and 30 for 1996 and 1998 with 28 and 34 degrees of freedom, respectively. This shows that the extended medium model fits the data as well as the best fit thin screen and is intuitively more appealing as it has only one free parameter. We note that incipient strong scattering causes a slight change in shape of the structure function as well as in time scale; hence we cannot use the differences in  $\chi^2$  to discriminate between the models.

The LSR is based on the motion of nearby stars and it may not be the best reference frame for the scattering plasma. Though differential Galactic rotation can be neglected over the 310 pc to the pulsar, we have to consider what is known about motion of the nearby interstellar gas. Current views of the “local bubble” are described in the proceedings of IAU colloquium 166 (Breitschwerdt et al 1998). This ionized region within 100-200pc of the Sun must largely determine the radio scattering for our pulsar observations. However, the basic idea of a hot ionized low density cavity has been refined by various recent measurements. Lallement (1998) discusses measurements of local interstellar “cloudlets” within a few pc of the Sun moving at 5-10 km s<sup>-1</sup> with respect to the LSR. Génova et al. (1998) describe the kinematics of gas within the bubble using various tracers. The velocity of particular clouds are reported as much as 20 km s<sup>-1</sup> relative to the LSR; though it is not clear how these are related to the motion of the radio scattering plasma which may extend along much of the line of sight.

Since these studies show a range of possible velocities in the local ISM, we considered a model in which the scattering medium is uniformly distributed between the Earth and the pulsar, but is

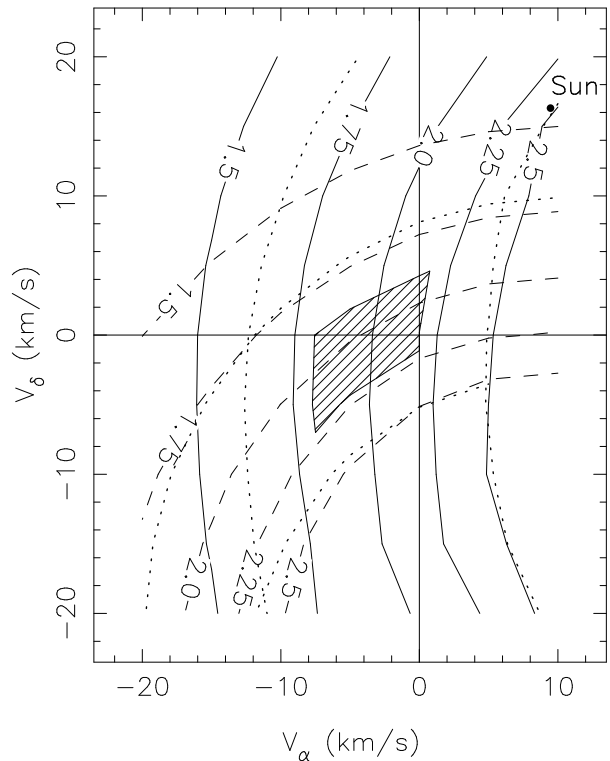


Fig. 6.— Scintillation time scale for observation in April 1996 (solid lines) and in October 1998 (dashed lines), calculated for a uniform scattering medium with a uniform velocity  $(V_\alpha, V_\delta)$  relative to the LSR. The time scales have been reduced by the factor 1.20 to account for the incipient strong scattering, as described in the text. The hashed region is where the computed time scales agree with the observations within  $\pm\sigma$  in both years.

moving with respect to the LSR at constant velocity  $(V_\alpha, V_\delta)$ . We performed an exhaustive search in velocity space for a single medium velocity that simultaneously matches the time scales 1996 and 1998 data. Here the measured time scales were obtained from the thin screen models fitted to the structure functions, since these models provided a good template for the observations.

We present the results in Figure 6 as contours of the predicted time scales (again reduced by the factor 1.2) in  $(V_\alpha, V_\delta)$  for the two observing periods. The hashed region shows where the calculated time scales lie within  $\pm\sigma$  of the measurements. Its extreme boundaries are  $-8 \leq V_\alpha \leq 1$  km s<sup>-1</sup> and  $-7 \leq V_\delta \leq 4$  km s<sup>-1</sup> and just include the LSR itself. The worst case errors due to uncertainties in the pulsar proper motion are shown by the dot-



ted contours, which increases the velocity range to  $-12 \leq V_\alpha \leq 5 \text{ km s}^{-1}$  and  $-16 \leq V_\delta \leq 7 \text{ km s}^{-1}$ . Since these are worst case limits the associated confidence level is 90%. It would clearly be interesting to tighten the proper motion estimate. We emphasize that this velocity only estimates the plasma motion in a plane normal to the direction toward the pulsar (at  $l = 140^\circ$ ,  $b = 31^\circ$ ) - plasma velocity along this direction is not constrained. Upon reflection, it seems remarkable that the simplest uniform Kolmogorov model (with only one parameter - the integrated strength of turbulence) provides a satisfactory match to both observations. We also note that the (projected) solar velocity in this frame lies nearly  $20 \text{ km s}^{-1}$  away and is clearly excluded.

To summarize, in the absence of other information about the nature of the scattering medium, we have two models that explain the observations. A uniform scattering medium which moves at nearly the LSR velocity and a local scattering region at a distance of about 195 pc which is stationary in the LSR. It is also evident that localized scattering regions at other distances would explain the observations if they were moving at the right velocity. We examine the tradeoff between distance and velocity in the context of other astronomical information about the local scattering environment in section 4.

### 3.3. Spectra with an Inner Scale

The possibility that the density spectrum is Kolmogorov but includes an ‘‘inner scale’’ at which damping becomes important, has been considered by several investigators (e.g. Coles et al. 1987, Romani et al. 1986, Spangler and Gwinn, 1990). The inner scale produces a rapid cutoff in the density spectrum which can be modelled with a gaussian multiplier of the form  $\exp[-\kappa^2 s_i^2/4]$ . The intensity spectrum is directly related to the density spectrum and shows the same multiplier. However, the structure function shows the effect much less dramatically - it changes exponent from  $D(s) \propto s^2$  to  $D(s) \propto s^{5/3}$  above  $s = s_i$  if  $s_i \ll r_f$ . We also note that both the screen and extended medium curves in Figure 2 approach the asymptotic 5/3 slope quite slowly; even the relatively steep thin screen model has only reached a slope of 1.44 at one tenth of the saturation level. Thus one should be quite cautious about interpreting the logarithmic slope of the structure functions at small lags as estimates of  $\alpha$ .

We used fits to the power spectra, rather than the structure function, to bound the inner scale. We

tested both the thin screen and uniform medium models described earlier. The best fit theoretical spectra for thin screen and uniform medium models are shown in Figure 3 as solid and dashed lines respectively. In 1996 all models with  $s_i < 6 \times 10^6 \text{ m}$  fit equally well, whereas in 1998 the fits at  $s_i = 2 \times 10^7 \text{ m}$  are significantly better. Although it is tempting to believe that an inner scale was detected in 1998, the detection depends on one or two points at the highest frequencies in the observed spectrum. These points are sensitive to the correction for system noise and intrinsic variation. We have assumed that both these corrections are white. A small amount of narrow band noise could significantly bias the highest frequency spectral estimates, increasing or decreasing them, depending on whether the noise is above or below the data range. Thus we have confidence only that the data indicate that  $s_i \lesssim 2 \times 10^7 \text{ m}$ .

The only astrophysical plasma with which we can make a comparison is the solar wind. There an inner scale has been well determined (Coles and Harmon 1989), and appears to be very close to the ion inertial scale, i.e. the Alfvén speed divided by the ion cyclotron frequency. Thus  $s_i = 684 (N_e \text{ cm}^{-3})^{-1/2} \text{ km}$  depends only on the density. At a typical density of  $N_e = 0.03 \text{ cm}^{-3}$  we have  $s_i = 4 \times 10^6 \text{ m}$ . Spangler and Gwinn (1990) made a similar suggestion for the dissipation scale in the interstellar plasma, and provided some evidence for inner scales  $\lesssim 10^6 \text{ m}$  for very heavily scattered lines of sight. It seems likely that the scattering takes place in regions of somewhat higher density than the mean interstellar medium, so it is likely that the inner scale is less than  $4 \times 10^6 \text{ m}$ . This is consistent with our observations but the bound is not very tight. The dynamic range of the observations would have to be increased by about an order of magnitude to provide a more interesting bound. An important consequence of the good spectral fits is to provide new and independent evidence in support of the Kolmogorov power law for the spectrum of plasma density in the local ISM; this has become the canonical model, but is not often tested critically.

### 3.4. Scintillation Index

In the foregoing analysis we have concentrated on interpreting the temporal variations characterized by the normalized structure functions. In weak scintillation the time scale depends only on the relative distribution of turbulence along the line

of sight, and is independent of its absolute level. We now estimate the absolute level of turbulence from the measured scintillation index and compare it with other observations of the same pulsar and also with models for the ISM electron density. The models describe the distribution of the variance of density, parameterized by  $C_N^2$ , the constant in equation (A12) for the density spectrum. But, in general, the observations can only estimate the integral of  $C_N^2$  along the line of sight, termed the scattering measure  $SM$ .

Observations of ISS have shown extreme variability in  $SM$  between even rather closely aligned sight lines. Previous workers (e.g. Cordes, Weisberg and Boriakoff, 1993 [CWB]; TC93) have modelled the distribution of  $C_N^2$  as a locally uniform background, with a stronger and more clumpy component superimposed. These models have been based primarily on pulsar measurements of the diffractive decorrelation bandwidth  $\delta\nu_d$  in strong scattering. Though this parameter is easy to estimate over 1-2 hours, the repeated 327 MHz observations of Bhat et al. (1999a) show it to be surprisingly variable. For many of the 20 pulsars observed within 1 kpc,  $\delta\nu_d$  varied by a factor of 5 or more over days to weeks. This variation is almost certainly caused by refractive scintillation, which modulates the diffractive spectrum and is caused by much larger scales in the ISM than those responsible for the diffractive scintillation itself. As noted by Cordes, Pidwerbetsky and Lovelace (1986), and by Gupta et al. (1994), the refractive modulations also tend to bias the apparent  $\delta\nu_d$  downwards, suggesting that the larger values of  $\delta\nu_d$  more accurately estimate the diffracting irregularities. With this preamble, we now compare  $SM$  derived from our scintillation index measurements with estimates based on  $\delta\nu_d$  measured for the same pulsar and also with  $SM$  from the TC93 and Bhat et al. (1998) models.

Our observations of the scintillation index give  $SM \sim 3 \times 10^{-6} \text{m}^{-20/3} \text{kpc}$ , depending slightly on whether we assume a screen or uniform scattering medium (see Table 1). Also listed are  $SM$  estimated from two  $\delta\nu_d$  observations (at 151 MHz by Rickett, 1970 and at 360 MHz by Cordes, 1986). We assume a uniform scattering medium in estimating  $SM$  from these measurements, and we noticed that Cordes (1986) used a formula higher by a factor 3.2 than that in TC93. As discussed in Appendix C, we use the formula in TC93, since it agrees with the independent analysis of Lambert and Rickett (1999).

Even with this correction, the 151 MHz observation gives an  $SM$  3.6 times higher than ours and the 360 MHz one is 13 times higher. The two measurements of  $\delta\nu_d$  differ by a factor 5 when scaled to a common frequency. From the discussion above, we may assume that the larger value of  $\delta\nu_d$ , i.e. the smaller value of  $SM$ , better represents the underlying density spectrum responsible for small scale ISS; but even then we have a factor of 3.5 discrepancy in  $SM$ . Both methods scale in the same way with screen distance and with pulsar distance, and so they cannot be reconciled by adjusting the distances in either the screen or uniform scattering geometries. In agreement with Bhat et al. (1999b), we conclude that we need a better understanding of the variability in  $\delta\nu_d$  observations; numerical simulations will be necessary, since the existing theory assumes asymptotically strong scattering which is not strictly applicable on the shorter paths to nearby pulsars.

We also calculated  $SM$  from the models of TC93 and Bhat et al. (1998). The former is 23 times and the latter is 18 times our estimate. TC93 model the plasma as uniform turbulence in the Galactic disk of 700 pc scale height in  $C_N^2$ . The recent model proposed by Bhat et al. (1998) adds detail near the Sun of a bubble of low turbulence surrounded by enhanced turbulence in a shell at 50-150 pc. They propose a range of ellipsoidal models for the shell, which the line-of-sight to PSR B0809+74 ( $l = 140^\circ, b = 31.6^\circ$ ) crosses at  $72 \pm 13$  pc from the Earth. The model specifies a low  $C_N^2$  inside the bubble, a value of  $SM$  for the shell and the same  $C_N^2$  as TC93 outside the shell. For our 310 pc path their shell contribution to  $SM$  dominates with 70% and the outer region provides 30% and the inner region less than 1%. Their model is closer to being a “screen” than a uniform extended scattering medium. Since we find 18 times lower  $SM$  than in their model, we conclude that the enhanced turbulent shell is not continuous and must have a hole toward pulsar B0809+74. We note that of the 20 pulsars observed by Bhat et al., the closest to PSR B0809+74 was PSR B0823+26 at the same Galactic latitude but 50 degrees away in longitude. Thus their observations are not in conflict with our low  $SM$  toward pulsar B0809+74.

The large  $SM$  discrepancies with the scattering models could be resolved by substantially reducing the pulsar distance. If  $L$  were reduced by a factor 5.5 it would bring our  $SM$  into line with that

| Observation                           | Frequency<br>(GHz) | Reference          | Model            | $SM$<br>( $m^{-20/3}kpc$ ) |
|---------------------------------------|--------------------|--------------------|------------------|----------------------------|
| $m_w = 0.8$                           | 0.93               | this work          | screen at 195 pc | $2.3 \times 10^{-6}$       |
| $m_w = 0.8$                           | 0.93               | this work          | extended med.    | $3.0 \times 10^{-6}$       |
| $\delta\nu_d = 0.95$ MHz <sup>a</sup> | 0.36               | Cordes(1986)       | extended med.    | $4.1 \times 10^{-5*}$      |
| $\delta\nu_d = 0.1$ MHz <sup>b</sup>  | 0.15               | Rickett(1970)      | extended med.    | $1.1 \times 10^{-5*}$      |
| Theory                                |                    | TC93               | extended med.    | $7.1 \times 10^{-5}$       |
| Theory                                |                    | Bhat et al. (1998) | shell of bubble  | $5.5 \times 10^{-5*}$      |

NOTE.—\*  $SM$  obtained using the formulae in Appendix C (and in TC93)

<sup>a</sup>average of observations at 0.36 and 0.41 GHz scaled to .36 GHz

<sup>b</sup> Value obtained from measurement of bandwidth that reduces scintillation index to 0.5, divided by 10 (see CWB)

from TC93 and bubble models. If that were the case, at 56 pc this would make PSR B0809+74 the closest pulsar to the Earth and the mean electron density  $0.1 \text{ cm}^{-3}$ , 3 to 5 times higher than other estimates. For example, PSR B0950+08 has a measured parallax distance of 130 pc and a mean electron density  $0.025 \text{ cm}^{-3}$ . Though the distance to B0809+74 may be uncertain by as much as 50%, it cannot be reduced by the factor 5.5, and we conclude that the turbulence level on this line of sight is much lower than described by either of the models. From our estimate of  $SM$  the effective average  $C_N^2$  toward B0809+74  $\sim 10^{-5} \text{ m}^{-20/3}$ . This is comparable to that in the inner cavity of the bubble model. It also agrees with that toward PSR B0950+08 ( $l = 229^\circ$ ,  $b = 44^\circ$ ) from the measurements of Phillips and Clegg (1992), after applying the correction factor from Appendix C. The low  $C_N^2$  for both of these pulsars suggests a quite large region of low turbulence in the hemisphere away from the Galactic center. The direction to our pulsar looks out from the local arm through an inter-arm region, which we suggest may have a lower plasma density than that described by the TC93 model. The low density might also be related to the local bubble, except that the X-ray observations of Snowden (1990) indicate that the bubble terminates between 50 and 100 pc towards PSR B0809+74.

#### 4. Discussion

We have found that the observations agree with the predictions for a Kolmogorov density spectrum in either a uniformly extended scattering medium moving at close to the LSR velocity or in screen at rest in the LSR, located in the range 170 – 220 pc from the Earth. We now consider whether these results are consistent with other ideas about the local

scattering environment.

In the local bubble model of Bhat et al. (1998), enhanced scattering is expected at  $72 \pm 13$  pc from the Earth. This is marked on Figure 4 by a rectangular bar and is clearly inconsistent with the screen solution near 195 pc. If the scattering region were located at 72 pc and co-moving with the LSR, the predicted time scale would be about 30% longer than observed in 1996 and twice as long as observed in 1998. Consequently, we also examined screen models with a fixed position and a free velocity  $\mathbf{V}_{scr}$  relative to the LSR.

We have measured weak scintillation time scales ( $\tau_{w96}$  and  $\tau_{w98}$ ) for two epochs. If  $x = z_o/L$  denotes the fractional distance to the screen, then the results of Appendix A give  $\tau_w = 0.98 \sqrt{\lambda L x(1-x)}/2\pi/|(1-x)\mathbf{V}_o + x\mathbf{V}_p - \mathbf{V}_{scr}|$ . With  $\mathbf{V}_o$  appropriate for the two epochs there are two equations, from which two possible solutions for  $\mathbf{V}_{scr}$  can be found at a given  $x$ . In Figure 7 these two velocity solutions are plotted as partial ellipses (solid and dashed lines), annotated with sample distances. The LSR velocity of a screen necessary to match the two observed time scales is thus given by a vector from the origin to the appropriate point on either curve. The lower velocity solutions are shown with sample error ellipses corresponding to the uncertainties in the time scale estimates. There are also errors due to uncertainty in the pulsar proper motion, given moving the point P by  $\pm 10 \text{ km s}^{-1}$  in either coordinate. These map in a non-linear fashion into an error in  $\mathbf{V}_{scr}$ , which is  $\sim 10 \text{ km s}^{-1}$  for screens near the pulsar, decreasing for screens nearer the Earth.

A screen at the proposed bubble distance of 72 pc needs a particular velocity of  $V_\alpha = -13.8 \pm 3$ ,  $V_\delta = 9.4 \pm 4 \text{ km s}^{-1}$  transverse to the pulsar line of sight. While this is a reasonable interstellar velocity, the problem remains that our estimate of  $SM$  is 18

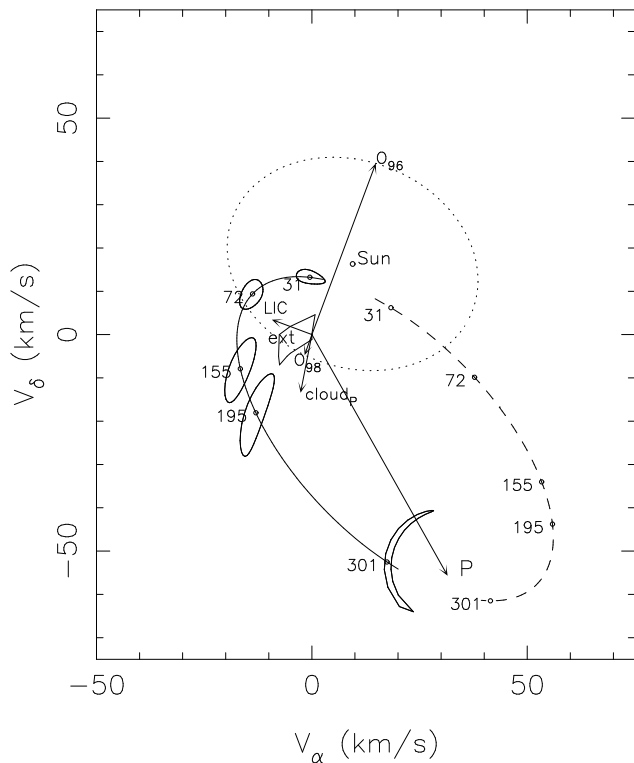


Fig. 7.— Velocities relative to the LSR, projected on the plane normal to the line of sight toward pulsar B0809+74. The pulsar velocity is marked by P. The Earth’s velocity is shown for the observations in 1996 and 1998, lying on the dotted ellipse of the Earth’s annual track, centered on the solar velocity. For each observation the line of sight cuts through the medium at a velocity that lies on a line between the Earth and pulsar velocities. “ext” marks  $1\sigma$  region of allowed velocity for a uniform scattering medium that best matches the data. Screen models give pairs of solutions for the screen velocity, which follow partial ellipses. One solution is drawn dashed since its larger velocities make it less likely. At 5 screen distances error contours are drawn for the allowed screen velocity. The plot does not include errors due to uncertainties in the proper motion. Also shown are the projected velocities of two relevant interstellar clouds in the solar neighborhood as discussed in the text.

times smaller than in the Bhat et al. model. The solution from section 3.1 with a screen near 195 pc requires the velocity  $V_\alpha = -13 \pm 4$ ,  $V_\delta = -18 \pm 10$  km s<sup>-1</sup> indicated by the elongated error ellipse, rather than being at rest in the LSR. We have also marked as a parallelogram the (modest) velocity

needed for scattering uniformly extended along the entire line of sight. The pulsar B0809+74 happens to lie at high ecliptic latitude and so the projected earth velocity (shown by the dotted ellipse in Figure 7) samples a large region of velocity space. It is likely that we can further constrain the scattering region by a series of weak ISS measurements at 2-3 month intervals over the year.

Figure 7 is also useful for displaying other velocity measurements of the local ISM, two of which we have projected onto our line of sight and plotted as vectors. The arrow marked LIC is the projected LSR velocity of the local interstellar cloud observed to be entering the heliosphere from its backscattered Lyman alpha (see Lallement, 1998). This cannot be related to the bubble solution with a comparable velocity, since the bubble model has no scattering nearer than about 70 pc. Génova et al. (1998) report measurements of Na I absorption lines over a wide range of galactic longitudes. They identify an interstellar cloud with velocity of 13.8 km s<sup>-1</sup> (toward  $l = 225^\circ$ ,  $b = 5.4^\circ$ ) covering a large solid angle including PSR B0809+74. The arrow marked “Cloud P” is the projected velocity of this interstellar cloud, which is comparable to that of our sample screen solution at 195 pc. Génova suggests (private communication 1999) that it may be a large warm diffuse cloud that extends 70 to 120 pc. Of course the other question in such a comparison is that the optical absorbing cloud may not be physically the same as the ionized region of enhanced turbulence. We also note that the likely interstellar plasma velocities are relatively small. The Alfvén speed in the warm ionized medium, which is assumed to be responsible for the scattering, is thought to be about 10 km s<sup>-1</sup>, similar to that of cloud motions.

Britton et al. (1998) have compared the angular scattering of pulsars with their temporal broadening and concluded that the scattering is often close to the pulsar. They suggest that it may be due to a nebula associated with each pulsar. This scenario cannot explain our observations of B0809+74, primarily because it is thought to be relatively old, of order  $T = 10^8$  yrs. If the scattering takes place at a distance R from the pulsar then the velocity of the scattering nebula  $V_{neb}$  with respect to the pulsar must be less than  $R/T$ . This is a very tight bound and such low velocities would produce much longer time scales than we observe. For example if  $R = 10$  pc, then  $V_{neb} < 0.1$  km s<sup>-1</sup>. However from Figure 7 we can see that a screen at a distance  $L - R = 301$  pc

from the Earth must be moving at 12 to 14 km s<sup>-1</sup> with respect to the pulsar to explain our measured time scales. For scattering near the pulsar the time scale can be approximated by  $\tau'_w = 0.82T/\sqrt{kR}$ , which is 250 hrs at R = 10 pc. Evidently a model of scattering near the pulsar would only be tenable only if the age of B0809+74 were less than  $0.6 \times 10^6$  yrs.

Our results can also be used to predict the interstellar scintillation for extragalactic sources B0716+714 and B0836+710, which are within 5° of B0809+74. Evidently, the predictions depend on whether or not we extrapolate the low level of scattering that we measure over 0.3 kpc out over the entire 1 kpc pathlength of the TC93 model.

For example B0716+714 is known to show rapid optical and radio variations (Wagner et al. 1996). The optical variations cannot be due to ISS and so imply a very small optical size; if this same size applied at cm wavelengths then it must also scintillate as an effective point source in the interstellar medium. Extrapolating our low  $C_N^2$  over the entire pathlength of the TC93 model, we predict  $m_w \sim 0.4$ , and spatial scale  $\sim 7 \times 10^8$  m at 5 GHz. Because the transverse LSR velocity of the earth varies considerably in this direction, the associated time scale  $\tau_w$  would vary from 50 hrs in October to 5 hrs in April. With the higher  $C_N^2$  level in the TC93 model the point source  $m_w \sim 2.1$ , indicating strong scintillation, which would split into diffractive and refractive components; however, their spatial and temporal scales would not be very different from the estimates above. A more realistic source model would include a maximum brightness (minimum angular size), which would reduce the rms flux variation and increase the time scales; nevertheless the strong annual variability in time scale would remain, if the scattering plasma does indeed share the motion of the LSR out to 1 kpc.

The source B0836+710 is known to have a very compact component from 20 GHz VLBI observations (Otterbein et al., 1998). If the diameter observed at 20 GHz applied at 5 GHz, it should also show interstellar scintillations, which are not observed (Quirrenbach, et al., 1992). However, at 5 GHz the compact component appears to be self-absorbed, so predicting the expected scintillation index versus frequency will require a full model for the source structure versus frequency.

## 5. Conclusions

We have developed a method for observing multiple epochs of weak scintillation of nearby pulsars whose proper motion has been measured. Our observations for pulsar B0809+74 can be explained by a uniform distribution of plasma “turbulence” which is stationary in the LSR. The density spectrum follows Kolmogorov law for scales between  $2 \times 10^7$  m and  $10^9$  m, i.e. the turbulence may have an inner scale  $\lesssim 2 \times 10^7$  m. This bound is consistent with the hypothesis that the inner scale is the ion inertial scale, which would be about  $4 \times 10^6$  m for an electron density of  $0.03 \text{ cm}^{-3}$ . The velocity of the scattering medium that best fits the observations is in the range  $-12 \leq V_\alpha \leq 5 \text{ km s}^{-1}$  and  $-16 \leq V_\delta \leq 7 \text{ km s}^{-1}$ . The error bounds, which are dominated by error in the pulsar proper motion, include the LSR.

The scintillation is also consistent with scattering from a localized region which is not stationary in the LSR, but this appears to be less likely for two reasons. First the scattering is considerably weaker than predicted by models of the distribution of turbulence in the local neighbourhood, so it is unlikely that the line of sight to B0809+74 is dominated by a local intensely scattering region. Second, if the scattering is dominated by a local region, it must be moving at a substantial velocity with respect to the LSR as shown in Figure 7. While this is possible, it appears to be somewhat less likely. The scintillation is not consistent with scattering in a “nebula” associated with the pulsar because the time scale of the scintillation is too short by several orders of magnitude.

The authors would like to acknowledge the help of Michael Kramer who pointed out that pulsar B0809+74 has a substantial polarization. This led to a reanalysis that significantly changed the conclusions and improved this paper. We thank the director and Staff of EISCAT for the use of the Sodankylä Telescope and we thank the NSF for partial support under grant AST 94-14144.

### A. Weak Scintillation Theory

We give here the theory of weak interstellar scintillation of a point source (pulsar) moving with respect to a scattering medium observed by a moving observer. Since the scattering is weak we can calcu-

late the contribution of a single thin screen and use the Born approximation to add the effect of many thin screens linearly.

Consider a thin phase screen between a point source P and an observer O. The screen is at distance  $z_p$  from P and  $z_o$  from O with  $z_o + z_p = L$ . The screen introduces a phase change  $\phi(\mathbf{s}_1)$  at transverse coordinate  $\mathbf{s}_1$ . Then the Fresnel diffraction integral for the complex field at an observer  $(0,0,L)$  can be written:

$$f(0,0,L) \simeq \frac{jk}{2\pi z_e} \exp[-jkL] \int d^2 \mathbf{s}_1 \exp \left[ j\phi(\mathbf{s}_1) - j \frac{k s_1^2}{2z_e} \right] \quad (\text{A1})$$

where  $z_e$  is defined by  $1/z_e = 1/z_o + 1/z_p$  and  $k$  is the radio frequency propagation constant. The factor  $jk/2\pi z_e$  ensures that the field has unit average intensity ( $\langle f f^* \rangle$ ) at  $z = L$ .

If now we consider the effect of moving the source to a transverse coordinate  $\mathbf{s}_p$  and the observer to  $\mathbf{s}_o$ , which are small compared to  $z_p$  and  $z_o$ , the field can be expressed as:

$$f(\mathbf{s}_p, \mathbf{s}_o, L) \simeq \frac{jk}{2\pi z_e} \exp[-jkL + j\Phi(\mathbf{s}_p, \mathbf{s}_o)] \times \int d^2 \mathbf{s}_1 \exp \left[ j\phi(\mathbf{s}_1) - j \frac{k |\mathbf{s}_1 - \mathbf{s}_{\text{eff}}|^2}{2z_e} \right] \quad (\text{A2})$$

Here

$$\Phi(\mathbf{s}_p, \mathbf{s}_o) = k |\mathbf{s}_p - \mathbf{s}_o|^2 / 2L \\ \mathbf{s}_{\text{eff}} = \mathbf{s}_p z_o / L + \mathbf{s}_o z_p / L, \quad (\text{A3})$$

where  $\mathbf{s}_{\text{eff}}$  is the transverse coordinate where a straight line from P to O intersects the screen.

From eq (A2) we can find the intensity  $I(\mathbf{s}_p, \mathbf{s}_o, L) = f f^*$  as a double integral. We need the intensity covariance

$$R_I^s(\boldsymbol{\sigma}_p, \boldsymbol{\sigma}_o, L) = \langle I(\mathbf{s}_p, \mathbf{s}_o, L) \times I(\mathbf{s}_p + \boldsymbol{\sigma}_p, \mathbf{s}_o + \boldsymbol{\sigma}_o, L) \rangle \quad (\text{A4})$$

Substituting the double integral form of  $I$  into the above equation generates the ensemble average of a quadruple integral over transverse screen variables  $(\mathbf{s}_1, \mathbf{s}_2, \mathbf{s}_3, \mathbf{s}_4)$ . After transforming to variables which are the various sums and differences of these and performing two integrations we obtain the spatial covariance

$$R_I^s(\boldsymbol{\sigma}_p, \boldsymbol{\sigma}_o, L) = \frac{k^2}{(2\pi z_e)^2} \int d^2 \mathbf{r} \int d^2 \mathbf{q} \exp \left[ -0.5 D_4(\mathbf{r}, \mathbf{q}) - \frac{jk}{z_e} (\mathbf{r} \cdot \mathbf{q} + \boldsymbol{\sigma}_{\text{eff}} \cdot \mathbf{q}) \right] \quad (\text{A5})$$

where  $\mathbf{r} = (\mathbf{s}_1 + \mathbf{s}_2 - \mathbf{s}_3 - \mathbf{s}_4)/2$  and  $\mathbf{q} = (\mathbf{s}_1 - \mathbf{s}_2 + \mathbf{s}_3 - \mathbf{s}_4)/2$  and  $D_4(\mathbf{r}, \mathbf{q}) = D(\mathbf{r}) + D(\mathbf{r}) - 0.5D(\mathbf{r} + \mathbf{q}) - 0.5D(\mathbf{r} - \mathbf{q})$  and  $\boldsymbol{\sigma}_{\text{eff}}$  is defined in an equation analogous to A3. Here the function  $D(\mathbf{r})$  characterizes the phase screen by the structure function of its phase at offset  $\mathbf{r}$ . Standard analysis of a plane wave normally incident on a phase screen gives the correlation function for intensity at spatial offset  $\mathbf{s}$  at a distance  $z$  from the screen (e.g. equation (5.3) of Tatarskii and Zavorotnyi, 1980). Equation (A5) is related to this simpler result by replacing  $\mathbf{s}$  by  $\boldsymbol{\sigma}_{\text{eff}}$  and  $z$  by  $z_e$ . A general treatment for waves scattered by such a screen requires a separate analysis for weak and strong scintillation. Under weak scintillation the important regions in  $\mathbf{r}$  and  $\mathbf{q}$  that dominate the integrations are where  $D_4$  is small compared to one, and  $\exp[-0.5D_4]$  can then be expanded to first order and integrated over  $\mathbf{r}$ . The result is often called the Born approximation [e.g equation (4.11) of Prokhorov et al. (1975)].

We are concerned with temporal variations caused as the observer moves at velocity  $\mathbf{V}_o$  and the pulsar moves at  $\mathbf{V}_p$ , both velocities with respect to the screen. The observer measures a temporal correlation function at time offset  $\tau$ , which is given by:

$$R_I^t(\tau) = R_I^s(\boldsymbol{\sigma}_p = \mathbf{V}_p \tau, \boldsymbol{\sigma}_o = \mathbf{V}_o \tau, L) \quad (\text{A6})$$

The associated structure function is

$$D_I^t(\tau) = 2R_I^t(0) - 2R_I^t(\tau) \quad (\text{A7})$$

The weak scintillation Born approximation gives:

$$R_I^t(\tau) = \int d^2 \boldsymbol{\kappa} P_\phi(\boldsymbol{\kappa}) 4 \sin^2(\boldsymbol{\kappa}^2 z_e / 2k) \times \exp[-j \boldsymbol{\kappa} \cdot \mathbf{V}_{\text{eff}} \tau] \quad (\text{A8})$$

Here  $P_\phi(\boldsymbol{\kappa})$  is the spectrum of the phase introduced by the screen (ie for a normally incident plane wave) at wavenumber  $\boldsymbol{\kappa}$ , which corresponds to  $(k\mathbf{q}/z_e)$  in the notation used above, and

$$\mathbf{V}_{\text{eff}} = \mathbf{V}_o z_p / L + \mathbf{V}_p z_o / L \quad (\text{A9})$$

which is the effective velocity of the point where a straight line from the pulsar to the observer intersects the screen. Note also that the low-wavenumber approximation in strong scattering is also given by this result with an extra exponential factor inside the integral  $\exp[-D(\boldsymbol{\kappa} z_e / k)]$ . For a layer of thickness  $\Delta$ , we replace  $P_\phi(\boldsymbol{\kappa})$  by  $P'_\phi(\boldsymbol{\kappa})\Delta$ , where

$$P'_\phi(\boldsymbol{\kappa}) = 2\pi r_e^2 \lambda^2 P_{N_e}(\kappa_x, \kappa_y, \kappa_z = 0, z_o) \quad (\text{A10})$$

where  $\lambda = 2\pi/k$  and  $P_{N_e}(\kappa_x, \kappa_y, \kappa_z, z_o)$  is the three-dimensional power spectrum of the electron density in the layer at a distance  $z_o$  from the observer. If  $P'_\phi(\boldsymbol{\kappa})$  is isotropic we obtain

$$D_I^t(\tau) = 32\pi^2 r_e^2 \lambda^2 \Delta \int_0^\infty \kappa d\kappa P_{N_e}(\kappa, z_o) \times \sin^2(\kappa^2 z_e / 2k) [1 - J_0(\kappa |V_{\text{eff}}| \tau)]. \quad (\text{A11})$$

This equation is used to compute models for comparison with the observations in section 3. With a simple power law density spectrum,

$$P_{N_e}(\kappa, z_o) = C_N^2(z_o) \kappa^{-\beta} \quad (\text{A12})$$

$$\beta = 11/3, \quad \alpha = \beta - 2,$$

the observed temporal structure function can be expressed as

$$D_I^t(\tau, z_o) = 2m_w^2 d_{\text{scr}}(\rho) \quad (\text{A13})$$

where

$$d_{\text{scr}}(\rho) = g_\alpha \int_0^\infty y^{-1-\alpha} \sin^2(y^2/8) \times [1 - J_0(y\rho/2)] dy \quad (\text{A14})$$

$$\rho = \tau V_{\text{eff}} \sqrt{k/z_e(z_o)}$$

$$g_\alpha = \frac{\alpha^{2+1/\alpha} \Gamma(1/2 + \alpha/4)}{\sqrt{\pi} \Gamma(1 - \alpha/4)}$$

With these definitions  $d(\infty) = 1$ , and for the Kolmogorov spectrum ( $\alpha = 5/3$ ), we find  $d_{\text{scr}}(0.99) = 0.5$  and so the scintillation time scale is  $\tau_w = 0.98 \sqrt{z_e/k} / V_{\text{eff}}$ , and  $g_\alpha = 7.346$ . We also give expressions for the scintillation index in terms of the screen coherence scale  $s_{\text{scr}}$  as

$$m_w^2 = \frac{\pi\alpha/4}{\Gamma(1 - \alpha/2) \sin(\pi\alpha/4)} \times \left[ \frac{2\sqrt{z_e(z_o)/k}}{s_{\text{scr}}} \right]^\alpha \quad (\text{A15})$$

$$s_{\text{scr}}^{-\alpha} = 8\pi^2 r_e^2 \lambda^2 C_N^2(z_o) \Delta \times \frac{\Gamma(1 - \alpha/2)}{\alpha^2 \Gamma(1 + \alpha/2)}$$

Here the coherence scale for the screen  $s_{\text{scr}}$  is defined as the lateral spatial offset over which there is an rms difference of 1 radian in the screen phase.

For an extended medium in weak scintillation we find  $D_I^t(\tau)$  by simply integrating along the line of sight, where the screen thickness  $\Delta$  becomes  $dz_o$ .

We proceed by assuming the medium to be “frozen” and refer  $\mathbf{V}_o$  and  $\mathbf{V}_p$  to the rest frame for the medium. In completing the integral, we assume that  $C_N^2$  is independent of  $z_o$  but include the  $z_o$  dependence of the other variables:

$$D_I(\tau, V_p, r, \theta_p) = \int_0^L D_I^t(\tau, z_o) dz_o / \Delta$$

$$z_e(z_o) = z_o(L - z_o) / L \quad (\text{A16})$$

$$V_{\text{eff}}(z_o) = V_p [z_o^2 + 2z_o(L - z_o)r \cos \theta_p + (L - z_o)^2 r^2]^{1/2} / L$$

The net effect is that each screen of thickness  $dz_o$  contributes with a different time scale to the total signal. This rounds the abrupt transition to saturation that is found in the thin screen. The variation of  $V_{\text{eff}}$  is determined by  $r = V_o/V_p$  and  $\theta_p$  the angle between  $\mathbf{V}_p$  and  $\mathbf{V}_o$ . Thus the detailed shape of the resulting structure function depends on the parameters  $r$  and  $\theta_p$ . At one extreme equal and parallel velocities ( $r = 1, \theta_p = 0$ ),  $V_{\text{eff}}$  is independent of distance and the structure function is just a stretched version of  $d_{\text{scr}}$ . In the case of anti-parallel velocities  $V_{\text{eff}}$  covers a wide range since there will be a distance at which it goes to zero and the corresponding time scale  $\tau_w \rightarrow \infty$ . In our application we know the pulsar and observer velocities with respect to the Sun. Our basic model assumes that the medium (either screen or uniform extended medium) moves with the local standard of rest. But the theory can equally be applied to models with the medium in uniform motion, if  $\mathbf{V}_p$  and  $\mathbf{V}_o$  represent the velocities with respect to the medium.

## B. Error in Structure Function Estimates

We need an expression for the errors expected in estimates of the structure function, in terms of the time lag  $\tau$  and duration of the data sequence  $T$  and the characteristic time constant for the process  $\tau_o$ . We present here an analytical solution and a simulation. The estimator used can be written in continuous (symmetrical) form as

$$\hat{D}(\tau) = \int_{-T'/2}^{T'/2} \Delta X(t, \tau)^2 dt / T' \quad (\text{B1})$$

where  $\Delta X(t, \tau) = X(t - \tau/2) - X(t + \tau/2)$  and  $T' = T - \tau$ . This estimator is unbiased as:

$$\langle \hat{D}(\tau) \rangle = \langle \Delta X(t, \tau)^2 \rangle = D(\tau), \quad (\text{B2})$$

which is independent of  $t$  or  $T$ . The covariance in the estimators at time lags  $\tau_1$  and  $\tau_2$  is then

$$\text{Cov}[\hat{D}(\tau_1), \hat{D}(\tau_2)] = \langle \hat{D}(\tau_1)\hat{D}(\tau_2) \rangle - \langle \hat{D}(\tau_1) \rangle \langle \hat{D}(\tau_2) \rangle. \quad (\text{B3})$$

Substituting B1 and taking the ensemble average inside the integrals this yields

$$\begin{aligned} \text{Cov}[\hat{D}(\tau_1), \hat{D}(\tau_2)] &= \int_{-T'_1/2}^{T'_1/2} \int_{-T'_2/2}^{T'_2/2} \\ &\langle \Delta X(t_1, \tau_1)^2 \Delta X(t_2, \tau_2)^2 \rangle \\ &dt_1 dt_2 / T'_1 T'_2 - D(\tau_1) D(\tau_2), \end{aligned} \quad (\text{B4})$$

where  $T'_1 = T - |\tau_1|$  and a similar expression for  $T'_2$ . We follow the method used by Jenkins and Watts (1969, pp 412-3, - JW) and assume that  $\Delta X$  is a Gaussian random variable with zero mean. Using the well-known average of the product of four such variables, we obtain:

$$\begin{aligned} \text{Cov}[\hat{D}(\tau_1), \hat{D}(\tau_2)] &= \int_{-T'_1/2}^{T'_1/2} \int_{-T'_2/2}^{T'_2/2} \\ &2 \langle \Delta X(t_1, \tau_1) \Delta X(t_2, \tau_2) \rangle^2 dt_1 dt_2 / T'_1 T'_2. \end{aligned} \quad (\text{B5})$$

Following (JW), we change to sum and difference variables of integration. The region of integration becomes a parallelogram, over which the sum variable is directly integrable to give

$$\begin{aligned} \text{Cov}[\hat{D}(\tau_1), \hat{D}(\tau_2)] &= \\ &\int_0^{T''} 4\Gamma(r, u, v)^2 (T'' - |r|) dr / (T''^2 - v^2) \\ &- \int_0^v 4\Gamma(r, u, v)^2 (1 - |r|/v) dr / (T'' - v), \end{aligned} \quad (\text{B6})$$

where  $u = (|\tau_1| + |\tau_2|)/2$ ,  $v = ||\tau_2| - |\tau_1||/2$  and  $T'' = (T'_1 + T'_2)/2 = T - u$ , and

$$\begin{aligned} \Gamma(r, u, v) &= 0.5[D(r - u) + D(r + u) - \\ &D(r - v) - D(r + v)]. \end{aligned} \quad (\text{B7})$$

*Variance in structure function with power law behavior*

The interesting special case of the variance in  $\hat{D}(\tau)$  corresponds to  $v = 0$   $u = \tau$  and  $T'' = T'$ , for which the second integral in equation (B6) is zero. We proceed by considering the various asymptotic forms. For small lags,  $D$  increases (monotonically) with lag and saturates at  $D_\infty = 2\sigma_X^2$ . A characteristic time scale separates these regions and can be

defined as  $D(\tau_o) = 0.5D_\infty$ . There are limiting cases in which the observing sequence is long enough to include many independent variations ( $T \gg \tau_o$ ) and the opposite extreme ( $T \ll \tau_o$ ).

First, consider  $T \gg \tau_o$ . Then with  $T > \tau \gg \tau_o$ , the triangular weight in eq (B6) can be ignored and the upper limit of the integral can be extended to infinity:

$$\text{Var}[\hat{D}(\tau)] \sim (4/T') \int_0^\infty \Gamma(r, \tau, v=0)^2 dr. \quad (\text{B8})$$

This gives the expected behavior for rms errors in  $\hat{D}$  as proportional to  $\sqrt{\tau_o/T'}$ . At large lags  $\tau \gtrsim \tau_o$ ,  $D$  then approaches saturation and

$$\Gamma(r, \tau, v=0) \sim D_\infty - D(r) = 2R(r) \quad (\text{B9})$$

where  $R(r)$  is the covariance function is related to  $D(r)$  as indicated. When put back into equation(B8), the result is 4 times the variance in the conventional autocovariance estimator at zero lag  $\hat{R}(0)$ , using the standard formula given by JW equation (5.3.21) with lag equal zero. We can then see that the two methods for estimating  $\sigma_X^2$  have the same rms error. Having discussed the errors for large lags, we now address small lags  $\tau \ll \tau_o \ll T$ . Then  $\Gamma$  can be approximated as

$$\Gamma(r, \tau, v=0) \sim D''(r)\tau^2/2. \quad (\text{B10})$$

Hence we see that for small lags the rms error in  $\hat{D}(\tau)$  varies as  $\tau^2$ , for any well-behaved  $D(\tau)$  function.

To make further progress, we assume a particular form for  $D(\tau)$ . The cases of interest are where  $D$  is a power law  $\propto \tau^a$  for small lags, and we adopt the following simple model (with  $1 \lesssim a \lesssim 2$ )

$$D(\tau) = D_\infty \tau^a / (\tau_o^a + \tau^a). \quad (\text{B11})$$

We can use this in equation(B8) for values of  $r \gtrsim \tau$ , but the integral is not done simply. We have investigated the integral numerically and find the following to be a useful approximation which connects the behavior for  $\tau \lesssim \tau_o$  and  $\tau \geq \tau_o$ .

$$\hat{D}(\tau)_{\text{rms}} \sim D_\infty 2 \sqrt{\frac{\tau_o}{T}} \frac{\tau^2}{\tau_o^2 + \tau^2}. \quad (\text{B12})$$

The accuracy of this approximation is best judged from the simulations described below. The important point about this analysis is that for exponents  $a$  less than 2, as  $\tau$  decreases the error in  $D(\tau)$  decreases more quickly than  $D(\tau)$  itself, and so the



fractional error in  $\hat{D}$  decreases with small  $\tau$ , as illustrated in the simulations of Coles and Harmon (1989).

The second limiting condition to be discussed is when the duration  $T$  is short compared to  $\tau_o$ . Then the triangular weight in equation(B6) must be included. For the variance in  $\hat{D}$  we again set  $v = 0$  and since  $T \ll \tau_o$  we can approximate  $D(\tau) \sim D_\infty(\tau/\tau_o)^a$ . Approximating the integral for  $2 > a > 1.5$  gives

$$\hat{D}(\tau)_{\text{rms}} \sim D_\infty(\tau/T')^2(T'/\tau_o)^{2a}a. \quad (\text{B13})$$

This result when normalized by  $D(\tau)$  shows a fractional error varying  $\propto (\tau/T')^{2-a}$ , again decreasing with small  $\tau$ .

Eq.(B6) also allows us to consider the covariance of  $D$  estimates at lags  $\tau_1$  and  $\tau_2$ . Examining the influence of non-zero  $v$ , equation(B7) shows that as  $v$  increases from zero it only has a substantial influence when it is comparable to  $u$ . In other words the estimates are only independent when the difference in time lags is comparable to their mean. A consequence of this correlation between estimates of  $D$  is that one can estimate the exponent  $a$  with reasonable accuracy even with small time lags and data duration less than  $\tau_o$ .

To investigate the validity of the foregoing analysis and its approximations we have simulated random time series with a power law structure function, applied the structure function estimator and studied its error properties. The process was specified by its power spectrum which was  $P(f) = P_o[(1 + (f/f_o)^2)^{-(a+1)/2}]$ . This has a high frequency form  $\propto f^{-a-1}$ , and the corresponding structure function is  $\propto \tau^a$  for  $\tau f_o \ll 1$ .

We use the standard method of simulating the process in the frequency domain. Independent zero mean Gaussian random variables of variance  $P(f)/2$  are stored into the real and imaginary parts of the complex Fourier representation of the series. After making it an Hermitian spectrum, an FFT is used to obtain the (real) random variable  $X_n$  at time samples  $t_n$ . Figure B8(a) shows a single example with  $a = 5/3$  and  $0 < n < 4095$ . The turnover frequency is set low, to give over two decades with power law behavior; this correspond to sample interval of  $\tau_o/180$  and  $T = 23\tau_o$ . We applied the structure function estimator eq (1) to the time series, and repeated the process on each new realization of the time series. This was repeated to obtain many independent estimates  $\hat{D}(\tau)$ , whose mean

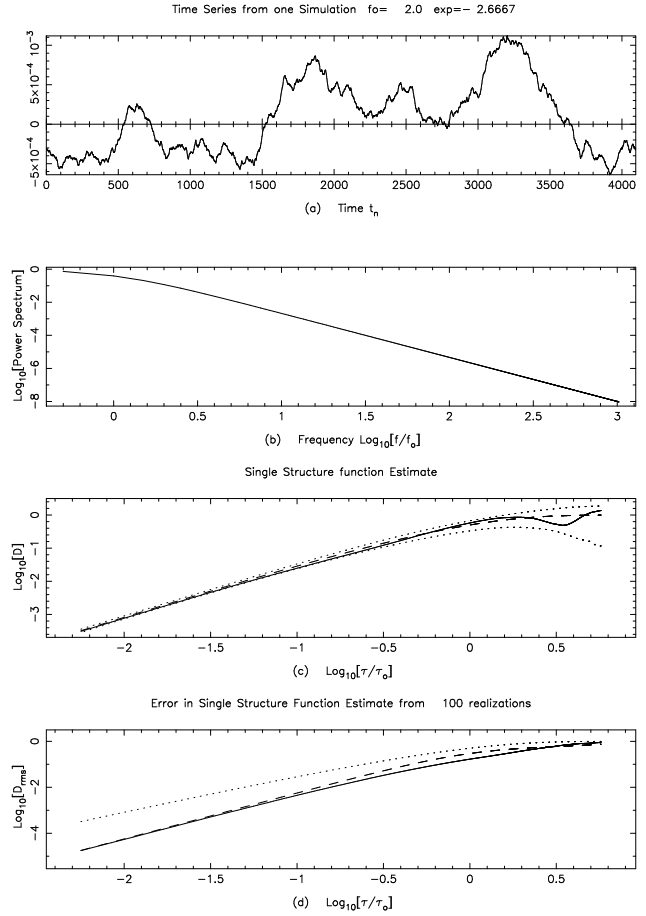


Fig. B8.— Simulation of a time series with a power law structure function ( $\propto t^{5/3}$ ). (a) Single sample of the time series (b) Ensemble average power spectrum. (c) Solid line is an estimate of the structure function from the single realization shown in (a); dashed line is the theoretical average structure function and dotted lines are plus and minus the standard deviation in the structure function estimate from (d). (d) Cumulated estimate of the rms error in the structure function estimates from 100 realizations (solid line); dashed line is the analytical approximation to the error given by equation (B12) dotted line shows the average structure function on the same scale, illustrating that the relative rms error in the estimate improves at small time lags.

and rms were computed versus  $\tau$ . In Figure B8(b), we show the ensemble average power spectrum; in Fig B8(c) we show as a heavy line an estimation  $\hat{D}$  from the single time series of Fig B8(a); the dashed line is the theoretical average  $D(\tau)$ ; the dotted lines show this mean plus and minus two standard devia-

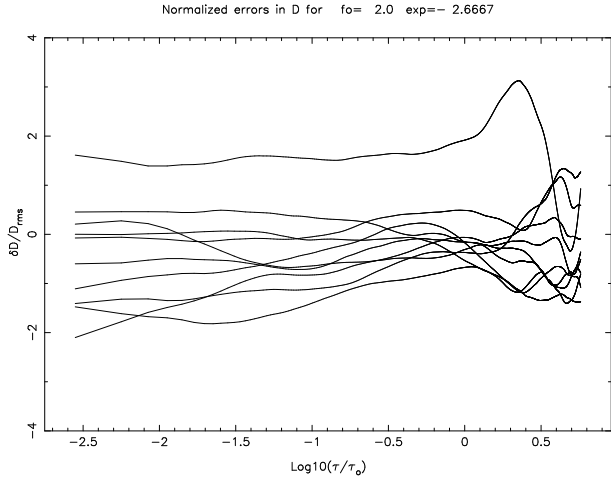


Fig. B9.— Simulation of a time series with a power law structure function ( $\propto t^{5/3}$ ). Set of 10 errors  $\hat{D}(\tau) - D(\tau)$  normalized by the expected error from equation (B12). This shows that for  $\tau$  less than about  $0.3 \tau_o$  the estimation errors are highly correlated, and that for lags above  $\tau_o$  the errors are correlated over a range in lag of about  $\tau_o$ .

tions derived from 50 realizations of  $\hat{D}$ . The fourth panel Fig B8(d) shows the cumulated estimates of the rms error in  $\hat{D}(\tau)$  as a solid line and the analytical approximation of equation(B12) as a dashed line, which evidently provides a very useful approximation to the error. The dotted line shows  $D(\tau)$  with the logarithmic scales it illustrates how the fractional error in  $\hat{D}$  becomes smaller for small  $\tau$ . The structure function estimates are plotted from 2 to 2048 sample intervals.

The degree of correlation between the  $\hat{D}$  estimates at two time lags, can be found as a function of the two lags. Instead of displaying such a correlation surface, we simply plot in Figure B9 a set of 10 errors  $\hat{D}(\tau) - D(\tau)$  normalized by the expected error from equation(B12). This shows that for  $\tau$  less than about  $0.3 \tau_o$  the estimation errors are highly correlated, and that for lags above  $\tau_o$  the errors are correlated over a range in lag of about  $\tau_o$ .

### C. Scattering Measure Estimates

For a screen of thickness  $\Delta$  at distance  $xL$  equations (A16) together give the relation of  $m_w^2$  to  $SM$ . With  $\alpha = 5/3$  this gives

$$SM = C_N^2 \Delta = 0.01465 \times m_w^2 [x(1-x)L\lambda/2\pi]^{-5/6} r_e^{-2} \lambda^{-2} \quad (C1)$$

For our measurements this gives  $SM \sim 2.8 \times 10^{-6} \text{m}^{-20/3} \text{kpc}$ , for a screen at 234 pc and (by coincidence) the same value for a screen at 72 pc (the edge of the bubble in the Bhat et al model). If, instead, we assume a uniform scattering medium, then

$$SM = 0.0664 m_w^2 (L\lambda/2\pi)^{-5/6} r_e^{-2} \lambda^{-2} \quad (C2)$$

and we obtain  $SM \sim 3.0 \times 10^{-6} \text{m}^{-20/3} \text{kpc}$  for our pulsar measurement.

$SM$  estimates were also been found by Cordes (1986), in which he measured the diffractive decorrelation bandwidth  $\delta\nu_d$  for various pulsars and converted to  $C_N^2$  for an equivalent uniform scattering medium. However, the formula used, his equation (6), derived by Cordes, Weisberg and Boriakoff (1993) [CWB] differs from those in the more recent model by TC93. For a spherical wave point source in a uniform scattering medium at distance  $L$  from the observer, the relation can be expressed in the general form based on CWB equation (6):

$$SM = A \nu^{\alpha+2} L^{-\alpha/2} \delta\nu_d^{-\alpha/2}. \quad (C3)$$

CWB derived  $A$  in their Appendix A and then increased it by a factor 6 to account for the effective line-of-sight weighting. Cordes (1986) used the resulting expression in deriving an average  $C_N^2 = SM/L$  for ISS measurements of over 70 pulsars. However, in constructing their model for the distribution of dispersing and scattering electrons in the ISM, TC93 used a different formula (their equation 8). It is expressed in terms of the scatter broadening time, which they relate by  $\tau_s = (2\pi\delta\nu_d)^{-1}$  to the decorrelation bandwidth. Putting this into the same format as above, their formula corresponds to  $A = 6.3 \times 10^{-4}$  where  $SM$  is in the units  $\text{m}^{-20/3} \text{kpc}$ ,  $\nu$  is in GHz,  $L$  is in kpc and  $\delta\nu_d$  is in MHz. We note that this is about one third of the value ( $A = 0.002$ ) used by CWB and Cordes (1986). In the study of scattering in the local bubble Bhat et al. (1998) used this larger value also.

The work of Lambert and Rickett (1999) allows us to obtain an independent theoretical evaluation for  $A$ . They computed the spherical wave two-frequency “diffractive” correlation function for three spectral models, including the Kolmogorov spectrum. Asymptotically strong scattering was assumed in a uniform scattering medium, leading to computed intensity correlation functions, from which precise values of the decorrelation bandwidth

were obtained. These are given in terms of a normalized decorrelation width  $v_d$  for each spectrum model; the value  $v_d = 2.320$  was found for the Kolmogorov spectrum. The decorrelation bandwidth is then  $\delta\nu_d = \nu v_d s_{0s}^2 / (L\lambda/2\pi)$ . Here  $s_{0s}$  is the observed spherical wave field coherence scale, where the phase structure function equals one. It is related by standard formulae to  $SM$  (e.g. their equations 11 and 13). Eliminating  $s_{0s}$  we find:

$$A_{\text{ext}} = \frac{(2\pi v_d)^{\alpha/2} \Gamma(1 + \alpha/2) \alpha (\alpha + 1) 2^\alpha}{8\pi^2 \Gamma(1 - \alpha/2) r_e^2 c^{2+\alpha/2}}, \quad (\text{C4})$$

where  $c$  is the speed of light. With  $\alpha = 5/3$  and using the same units as above, we find  $A = 6.25 \times 10^{-4}$  in very close agreement with the formula used by TC93, and 0.315 times the value used in work following Cordes (1986) and CWB. When comparing observations and theory with an accuracy of better than a factor of 3, observers should use the constant  $A = 6.3 \times 10^{-4}$  in equation (C3). In particular, in the models of Bhat et al.  $C_N^2$  should be reduced by a factor of three over their published values. We have made the appropriate changes in listing SM values for pulsar B0809+74 in Table 1. For a screen at distance  $xL$  from the Earth, a similar analysis leads to:

$$A_{\text{scr}} = 0.179 A_{\text{ext}} [x(1-x)]^{-5/6} \quad (\text{C5})$$

## REFERENCES

- Backer, D. C. 1975, *ApJ*, 190, 395
- Bhat, N. D. Ramesh, Gupta, Y. & Rao, A. Pramesh 1998, *ApJ*, 500, 262
- Bhat, N. D. Ramesh., Rao, A. P., & Gupta, Y. 1999a, *ApJ*, 514, 249
- Bhat, N. D. Ramesh, Gupta, Y. & Rao, A. Pramesh 1999b, *ApJ*, 514, 272
- Britton, M. C., Gwinn, C. R. & Ojeda, M. J. 1998, *ApJ*, 501, L101
- Breitschwerdt, D., Freyberg, M. J. and Trümper, J. 1998, “The Local Bubble and Beyond”, *Proceedings of IAU Colloquium 166*, Ed. Breitschwerdt, D., Freyberg, M. J. and Trümper, J., p1
- Coles, W. A. & Harmon, J. K. 1989. *ApJ*, 227, 1023
- Coles, W. A., Frehlich, R. G., Rickett, B. J. & Codona, J. L. 1987. *ApJ*, 315, 666
- Cordes, J. M. 1986, *ApJ*, 311, 183
- Cordes, J. M., Weisberg, J. M. & Boriakoff, V. 1985, *ApJ*, 288, 221 [CWB]
- Cordes, J. M. & Rickett, B. J. 1998, *ApJ*, 507, 846
- Génova, R., Beckman, J. E. & Alamo, J. R. 1998, in “The Local Bubble and Beyond”, *Proceedings of IAU Colloquium 166*, Ed. Breitschwerdt, D., Freyberg, M. J. & Trümper, J., p 195
- Gould, D. M., Lyne, A. G., 1998, *MNRAS*, 301, 235
- Gupta, Y., Rickett, B. J., & Lyne, A. G. 1994, *MNRAS*, 269, 1035
- Jenkins, G. M. & Watts, D. G. 1969, “Spectral Analysis and its Applications” (San Francisco: Holden-Day)
- Lallement, R. 1998, in “The Local Bubble and Beyond”, *Proceedings of IAU Colloquium 166*, Ed. Breitschwerdt, D., Freyberg, M. J. & Trümper, J., p19
- Lambert, H. C. & Rickett, B. J. 1999, *ApJ*, 517, 299
- Lyne, A. G., Anderson, B. & Salter, C. J. 1982, *MNRAS*, 213, 613
- Malofeev, V. M., Shishov, V. I., Sieber, W., Jessner, A., Kramer, M. & Wielebinski, R., 1996, *A&A*, 308, 180
- Narayan, R. 1992, *Phil. Trans. R. Soc. London A*, 341, 151
- Otterbein, K., Krichbaum, T. P., Kraus, A., Lobanov, A. P., Witzel, A., Wagner, S. J., & Zensus, J. A. 1998, *A&A*, 334, 489
- Phillips, J. A. & Clegg, A. W. 1992, *Nature*, 360, 137
- Quirrenbach, A., Witzel, A., Krichbaum, T. P., Hummel, C. A., Wegner, R., Schalinski, C. J., Ott, M., Alberdi, A., & Rioja, M. 1992, 258, 279
- Prokhorov, A. M., Bunkin, F. V., Gochelashvily & K. S., Shishov, V. I. 1975. *Proc. I.E.E.E.* 63, 790
- Rickett, B. J. 1970, *MNRAS*, 150, 67
- Rickett, B. J. 1990, *ARA&A*, 28, 561
- Romani, R. W., Narayan, R., & Blandford, R. 1986, *MNRAS*, 220, 19
- Snowden, S. L. 1998, in “The Local Bubble and Beyond”, *Proceedings of IAU Colloquium 166*, Ed. Breitschwerdt, D., Freyberg, M. J. & Trümper, J., p103
- Spangler, S. R., & Gwinn, C. R. 1990, *ApJ*, 353, L29
- Tatarskii, V. I. & Zavorotnyi, V. U. 1980, *Progress in Optics*, 18, 207
- Taylor, J. H. & Cordes, J. M. 1993, *ApJ*, 411, 674
- Taylor, J. H., Manchester, R. N., & Lyne A. G. 1993, *ApJS*, 88, 529
- Wagner, S. J., Witzel, A., Heidt, J., Krichbaum, T. P., Qian, S. J., Quirrenbach, A., Wegner, R., Aller, H., Aller, M., Anton, K., Appenzeller, I., Eckart, A., Kraus, A., Naundorf, C., Kneer, R., Steffen, W., & Zensus, J. A. 1996, *AJ*, 111, 2187